J. Phys. B: At. Mol. Opt. Phys. **24** (1991) 1851–1866. Printed in the UK

Vibrationally resolved electron HeH^+ collisions using the non-adiabatic R-matrix method

Baljit K Sarpal†, Jonathan Tennyson† and Lesley A Morgan‡

† Department of Physics and Astronomy, University College London, London WC1E 6BT, UK

‡ Computer Centre, Royal Holloway and Bedford New College, Egham, Surrey TW20 0EX, UK

Received 25 October 1990

Abstract. We use the R-matrix formalism for the electron–molecule collision problem to calculate elastic scattering cross sections for the HeH^+ ion as a function of internuclear separation. Vibrationally resolved elastic and inelastic cross sections are obtained within the adiabatic and the non-adiabatic nuclei approximation. These calculations give cross sections of similar magnitude but the non-adiabatic results show complicated series of 'nuclear-excited Feshbach' resonances. The lowest $^2\Sigma$ resonances coincide with unexplained structures in the observed dissociative recombination cross section. We find that the vibrational excitation cross sections are considerably smaller than those calculated using the Coulomb–Born approximation, offering one explanation for why HeH^+ has not so far been detected in planetary nebulae.

1. Introduction

The study of electron scattering by HeH^+ is of considerable astrophysical significance due to its predicted presence in the cool plasmas found both in planetary nebulae and the interstellar medium (Roberge and Dalgarno 1982). The ion is expected to play an important part in the chemistry of these bodies. It is therefore imperative that one determines accurately the abundance and the mechanisms via which HeH^+ is removed from the reaction chain.

Due to the absence of any suitable curve crossings (Michels 1989) of the neutral molecule with potential energy curves of the ion, direct dissociative recombination (DR) is ruled out as a possible removal mechanism. It has thus been assumed that the DR cross section is negligibly small leading to HeH^+ in appreciable and observable concentrations (Roberge and Dalgarno 1982). However a recent study of the planetary nebula NGC 7027 (Moorhead *et al* 1988) failed to observe its infrared spectrum suggesting a significantly lower than expected abundance of HeH^+. This may be due to the neglect of DR or an overestimate of the populations of the excited vibrational levels. The major mechanism for the population of excited levels is vibrational excitation by electronic collisions. A recent experimental study (Yousif and Mitchell 1989) has indeed found appreciable DR and observed some unexpected structure in the DR cross section. In the absence of curve crossings this is only possible through the coupling of

0953-4075/91/071851+16$03.50

the nuclear motion with the electronic continuum. Such a mechanism would indicate the breakdown of the Born–Oppenheimer approximation.

The Born–Oppenheimer approximation has been one of the most useful concepts in the interpretation of molecular spectra. However for light molecules and low electron energies the partitioning of the wavefunction into electronic and nuclear components implied by the approximation may no longer be valid. This is particularly true in the region of resonance states. In such cases there may be considerable departures from the predictions of any theory which is built upon the Born–Oppenheimer approximation.

The adiabatic nuclei approximation assumes that the matrix elements of the nuclear kinetic energy operator be zero between the electronic wavefunction. Within such an approximation the nuclear and electronic part of the problem can be treated almost independently and perturbations in the vibrational excitation spectrum can be explained by reference to Franck–Condon overlap factors for electronic excitations and vibrationally averaged dipole moment for vibrational excitations. Indeed these have proved to be powerful concepts in molecular spectroscopy.

In this paper we study the modifications in the vibrational excitation cross section arising from a more rigorous treatment of the nuclear motion, including non-adiabatic effects. To do this we employ the multicentre, molecular R-matrix method which has been extended to include the non-adiabatic treatment of nuclear motion (Gillan *et al* 1987) introduced by Schneider *et al* (1979). This approach has been successfully applied to low-energy scattering of electrons by N_2 (Morgan 1984b), HF (Morgan and Burke 1988) and HCl (Morgan *et al* 1990). Morgan *et al* (1990) were able to show that the structure in the vibrational excitation of HCl, which is only evident when nuclear motion is treated non-adiabatically, was due to 'nuclear-excited Feshbach' resonances i.e. due to the presence of a bound state of the HCl^- ion. These states are uncommon in neutral molecules with subcritical dipole moments, however for positive ions such electronic capture states form Rydberg series converging to the ionic target state. For this reason non-adiabatic effects are expected to be more pronounced for positive ions, and these may be further enhanced if the molecule consists of light nuclei.

DR cross sections are notoriously difficult to measure (Mitchell 1990), so an independent theoretical determination would appear important. As a prelude to DR calculations we report low-energy elastic and inelastic scattering results for the HeH^+ ion. We present vibrationally resolved cross sections which show considerable structure due to non-adiabatic effects. A modified Coulomb–Born calculation of the $v = 0 \rightarrow 1$ cross section by Boikova and Ob'edkov (1968) is the only previous calculation for HeH^+. To our knowledge non-adiabatic effects for this system, or indeed for any other molecular ion, have not so far been considered; see for example the studies on $e–H_2$ by Raseev and Le Rouzo (1983), Tennyson *et al* (1986) and Collins *et al* (1986).

2. Calculations

2.1. Target states

An accurate description of the scattering process is dependent on the ability to start with an accurate description of the initial state, i.e. the target states. We carried out a CI expansion of the lowest three target states ($X\ ^1\Sigma^+$, $a\ ^3\Sigma^+$ and $A\ ^1\Sigma^+$) from the Hartree–Fock (HF) orbitals generated by an SCF procedure (McLean 1971). The SCF orbitals were generated with the $7 \times 5B$ Slater-type orbital (STO) basis of Peyerimhoff

(1965)† which was augmented with π, δ and ϕ orbitals, having the same exponents as the Peyerimhoff set, see table 1. The full CI energies of the lowest three states are given in table 2 where they are compared with CI calculations of Green *et al* (1974) and Green *et al* (1978) who use a combination of STO and ellipsoidal orbitals.

Table 1. Exponents of the basis set, Peyerimhoff's 7 x 5B set augmented by π, δ and ϕ orbitals and retaining all components of the spherical harmonics.

Helium		Hydrogen	
Orbital	Exponent ζ	Orbital	Exponent ζ
1s	1.37643	1s	1.00949
1s′	3.87107	2s	1.18036
2s	1.54335	2s′	2.56229
2p	2.64576	2p	1.79089
2p′	3.24082	3d	2.41228
3d	2.54147		
4f	3.73526		

Table 2. Energy of the lowest singlet state (in Hartree) of HeH^+ and the lowest two excitation energies (in eV). The figures in square brackets denote the number of components of the CI wavefunction.

Level	Exact energy[a]	Our full CI		Our reduced CI	
$X\ ^1\Sigma$	−2.97649 (E_h)	−2.97565 (E_h)	[106]	−2.95120 (E_h)	[11]
$a\ ^3\Sigma$	21.75 (eV)	21.84 (eV)	[84]	21.67 (eV)	[6]
$A\ ^1\Sigma$	26.42 (eV)	26.52 (eV)	[106]	26.36 (eV)	[11]

[a] Green *et al* (1974, 1978).

Ideally one would like to use the best target representation available, however the number of components of the $(N+1)$-electron wavefunction for full CI states are prohibitively large for scattering calculations and a smaller CI expansion was found to be necessary. We found that an expansion with four σ and one π orbital was sufficient to yield accurate CI target energies for a range of nuclear geometries, see table 2 and figure 1. The fourth σ orbital was found to be necessary for correlating the ground state at large internuclear distances; without it the CI curve tended to the SCF curve for large internuclear separations. Our full CI target wavefunctions consist of 106 components for the singlet states and 84 components for the triplet state. The corresponding numbers for the reduced set are 11 and 6 respectively. It is the reduced CI model which we employ throughout this work.

Vibrationally resolved calculations were based on a grid of 13 geometries (R = 1.0, 1.2, 1.3, 1.4, R_e = 1.455, 1.5, 1.6, 1.8, 2.0, 2.4, 2.8, 3.0, 4.0 a_0). For the vibrationally resolved work described here the ground state potential energy curve was fitted to a Morse function and its eigenfunctions determined. This approximation is valid well away from the dissociation limit, as can be seen in figure 1. We considered the lowest six vibrational levels of the ground state; for these the Morse fit to our reduced

† Our calculation with the Peyerimhoff 4 x 2A basis agree with her published results, however our results with the 7 x 5B basis set are consistently higher than hers by $5 \times 10^{-5} E_h$.

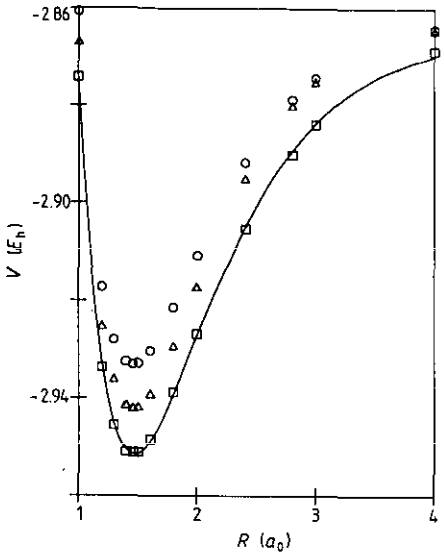

Figure 1. Potential energy curves for the ground state X $^1\Sigma$. O, SCF; Δ, CI (3 σ orbitals); □, CI (4 σ orbitals), see text for definition. The curve is a Morse fit to the CI (4 σ) data.

CI potential energy curve resulted in vibrational thresholds at 0.38, 0.73, 1.03, 1.31 and 1.54 eV. These thresholds are in reasonable agreement with the more accurate vibrational level energies calculated by Dabrowski and Herzberg (1977); the agreement ranges from 0.01 eV for the lowest threshold and 0.1 eV for the highest threshold calculated. Although these results do not represent spectroscopic accuracy they are sufficient for our purposes and could only be improved by a considerable increase in the target expansion.

2.2. Inner region

The *R*-matrix approach and its application to electron–molecule scattering are well documented (Gillan *et al* 1987, Morgan 1990) and we omit a detailed discussion of the method. The *R*-matrix method relies on the ability to partition the configuration space into two region, namely the *inner* and *outer* regions. In the inner region, bounded by a sphere of radius a (in this work $a = 10\ a_0$), the problem is treated using quantum chemistry methods, in our case a modified version of the ALCHEMY molecular structure package (McLean 1971, Noble 1982). The inner region wavefunction is given by

$$\psi_k = \mathcal{A} \sum_{i,j} \phi_i(\boldsymbol{x}_1 \cdots \boldsymbol{x}_N) u_{ij}(\boldsymbol{x}_{N+1}) a_{ijk} + \sum_i \chi_i(\boldsymbol{x}_1 \cdots \boldsymbol{x}_{N+1}) b_{ik}. \qquad (1)$$

where ϕ_i is the target wavefunction discussed above and $N = 2$ for HeH^+. The continuum orbitals, u_{ij}, are expanded as a partial-wave expansion. The radial continuum functions are obtained by numerically solving the 1D Schrödinger equation using the isotropic part of the SCF potential. The continuum orbitals are then Schmidt orthogonalized to the occupied and virtual SCF molecular orbitals. We included continuum orbitals having $l \leq 5$ and energies less than 10 Ryd. The whole calculation is repeated for each total symmetry; in this work symmetries with $m \leq 3$ were considered.

In (1), the functions χ are the $(N+1)$-electron correlation functions constructed from the virtual L^2 orbitals. We included the lowest six each of the σ and π orbitals, three δ and one ϕ orbitals. The orbitals used in the construction of the CI target can be used to allow for short-range polarization. The remaining orbitals are only used for correlation. This ensures that the $(N+1)$-electron states correctly converge onto the target states, i.e. the $(N+1)$-electron states are not overcorrelated with respect to the target states. The R-matrix is then constructed in the usual way (see Gillan *et al* 1987).

If nuclear motion is to be included ***ab initio*** , the vibronic wavefunction can be represented by

$$\theta_i = \sum_{jk} \psi_k(x_1 \cdots x_{N+1}; R)\eta_j(R)c_{ijk} \tag{2}$$

where ψ_k are the wavefunctions defined in equation (1). The basis, η_j, consists of orthogonal polynomials (we used 25 Legendre polynomials) and represents the nuclear motion wavefunctions. The total Hamiltonian, which includes the nuclear kinetic energy operator is diagonalized with respect to this new basis.

The non-adiabatic approximation is implemented by the method proposed by Schneider *et al* (1979). The fixed-nuclei R-matrix poles provide the potentials for an R-matrix treatment of the nuclear motion. This partitions the nuclear motion configuration space into two regions separated by a sphere $R = A$ (where R represents the nuclear separation). This defines a super R matrix on a hypersphere bounded by $r \leq a$ and $R \leq A$ and which is then treated in exactly the same manner as in the fixed geometry formalism (Gillan *et al* 1987).

Although the approach of Schneider *et al* (1979) is in principle less accurate than a full close-coupling calculation, convergence can be demonstrated by increasing the number of electronic and nuclear functions included explicitly in the super R matrix. This approach, like our fixed-nuclei calculations, makes no distinction between resonant and non-resonant contributions to the scattering process.

2.3. Outer region

Solution of the inner region problem yields the R matrix (or the super R matrix) on the R-matrix boundary. This is propagated (Morgan 1984a) to some suitably large radius where Gailitis asymptotic expansion techniques (Noble and Nesbet 1984) are used to give K matrices. Because of the low energies of the incident electrons in our calculations we found that it was necessary to propagate outwards to a large radius, 300 a_0, in order to achieve stable results for scattering in the non-adiabatic model. Despite this the non-adiabatic calculations actually proved computationally cheaper than the adiabatic ones because only one (as opposed to 13) R matrices need to be treated.

The adiabatic approximation, which assumes that the electronic part of the wavefunction is only parametrically dependent on R, is implemented by calculating the K matrix and then the T matrix for each fixed geometry. The T matrices are then numerically averaged over the nuclear geometries

$$T_{vv'} = \langle v|T(R)|v'\rangle \tag{3}$$

where integration over the R (internuclear separation) variable is implied. For our present discussion the collisions do not induce electronic excitations therefore the label

for electronic states has been dropped in (3) and hereafter. The target vibrational wavefunctions, $|v\rangle$ and $|v'\rangle$, are taken to be the eigenfunctions of the potential energy curve representing the target state. We included the six lowest vibrational levels of the ground state for the work described here.

The cross sections are given by

$$\sigma_{v\to v'} = \frac{\pi}{k_v^2}|T_{vv'}|^2 \tag{4}$$

where $\mathbf{T}$ is either the adiabatically averaged T matrix, (3), or the non-adiabatic T matrix and the subscript on k denotes the threshold relative to which the momentum is expressed.

The non-adiabatic treatment explicitly considered the ten lowest R-matrix poles for Σ and Π symmetries, and seven and five for the Δ and Φ symmetries respectively. Among these it is necessary to properly account for any pole crossings. We found that the seventh and eighth pole for the Σ symmetry underwent a crossing near $R = 1.4\ a_0$, this is very close to the equilibrium geometry of $1.455\ a_0$. This crossing was treated by diabatically continuing the curves and omitting the $R = 1.4\ a_0$ geometry from our R grid for this symmetry.

In this work we retained the ground state dipole and quadrupole moments in the multipole expansion of the outer region potential. We found that the final results are relatively insensitive to the multipole moments used in the potential expansion.

3. Results

3.1. Equilibrium geometry

As was remarked in section 2.1 we are limited to the number of L^2 functions we can include in the expansion (1). As well as requiring that the excitation energies of the ionic target be well reproduced, we require that the model also produces good scattering results. In order to test that the model we used was accurate we carried out several calculations for the equilibriums geometry $R_e = 1.455$.

Tennyson *et al* (1987) pointed out that, since the continuum basis is generated from the isotropic part of the SCF potential, the continuum orbitals may suffer from linear dependence with the virtual molecular orbitals included in the expansion of the wavefunction (1) in the internal region. This was considered to be a particular problem with ionic targets because of the attractive nature of the model potential. This linear dependence is revealed firstly in the orthogonalized molecular orbitals having large coefficients and secondly, more drastically, in the appearance of unphysical R-matrix poles. The linear dependence can be eliminated by Lagrange orthogonalization of the continuum orbitals to selected target orbitals (Tennyson *et al* 1987). The present calculations proved completely stable to Lagrange orthogonalization, therefore Schmidt orthogonalization was deemed sufficient.

In order to determine whether our scattering results have converged with respect to the partial-wave expansion we carried out a calculation at equilibrium geometry retaining partial waves with $l \leq 8$ and $m = 0$. It was found that the eigenphase sum was uniformly increased by about 1% over the entire energy region below the first vibrational threshold. We are therefore confident that retaining only the $l \leq 5$ partial waves will not result in any significant loss of accuracy.

Because one cannot rigorously examine the convergence of polarization configurations in the expansion (1) for CI targets, we checked that the eigenphase sum for our reduced CI model converged to that of the SCF target with short-range polarization (SEP) included via two-particle one-hole type excitations (Tennyson 1988). Because we are concerned with a strongly bound ionic target, consequently with a small polarizability, neglect of higher polarization configurations should not be significant, certainly for low-energy scattering. In the low-energy region, relevant for this work, the CI eigenphase sum agreed with the SEP eigenphase sum to within 3%. For high energies, around 10 eV, this agreement was 6%.

For $R = R_e$ we were able to calculate the 30 lowest bound states of symmetry up to Φ, for the neutral molecule using a modified version of the algorithm of Seaton (1985). Our energy separations for the lowest four states agreed with the theoretical calculations of Theodorakopoulos *et al* (1984) and experimental determinations of Ketterle (1989) to within 0.02 eV. The agreement with Ketterle (1989) is consistently better for energy differences between higher levels. A systematic study of these states, including nuclear motion effects, is currently in progress (Sarpal *et al* 1991).

3.2. Elastic scattering

In the low-energy elastic scattering channel the adiabatic results are very similar to the equilibrium geometry results, with the expected divergence of the cross section for a positive ion at zero energy, and monotonically decreasing for increasing electron energy. The elastic cross section displays the characteristic $1/E$ behaviour. The non-resonant elastic scattering is dominated by the Σ symmetry incident electrons. The cross section for Σ incident electrons is found to be 20 times higher than for Π electrons and 60 times higher than Δ electrons. This suggests that the elastic scattering cross section is rapidly convergent with Λ.

The eigenphase sum for the equilibrium geometry is very flat in the low-energy region. The situation is more interesting when nuclear motion is treated non-adiabatically, when we observe many resonances in the calculated eigenphase sum. Figure 2 shows the eigenphase sum for the four symmetries; note the change of vertical scale in the plots. Of course there is no concept of eigenphase sum for the adiabatic calculations. These resonances in the non-adiabatic eigenphase also show up as resonances in the elastic scattering cross section with Σ being the most dominant symmetry.

Previous work (Tennyson 1988) on scattering from CH^+ has shown complex multichannel quantum defects (MCQD) to be very useful for analysing complicated resonance structures. The T matrix just above a threshold can be used to calculate the MCQD parameters, $\mu \equiv \alpha + i\beta$ (Seaton 1983). The parameter α is related to the effective quantum number, n^*, by $\alpha = n - n^*$. The effective quantum number can be determined from the relation

$$E_{n,v} = E_{\infty,v} - \frac{1}{n^{*2}}$$

where $E_{n,v}$ and $E_{\infty,v}$ are energies (in rydbergs) of the neutral vibronic level and the relevant ionization limit for the same vibrational quantum number. The β parameter for a resonance is defined as

$$\beta = \frac{\Gamma n^{*3}}{4}$$

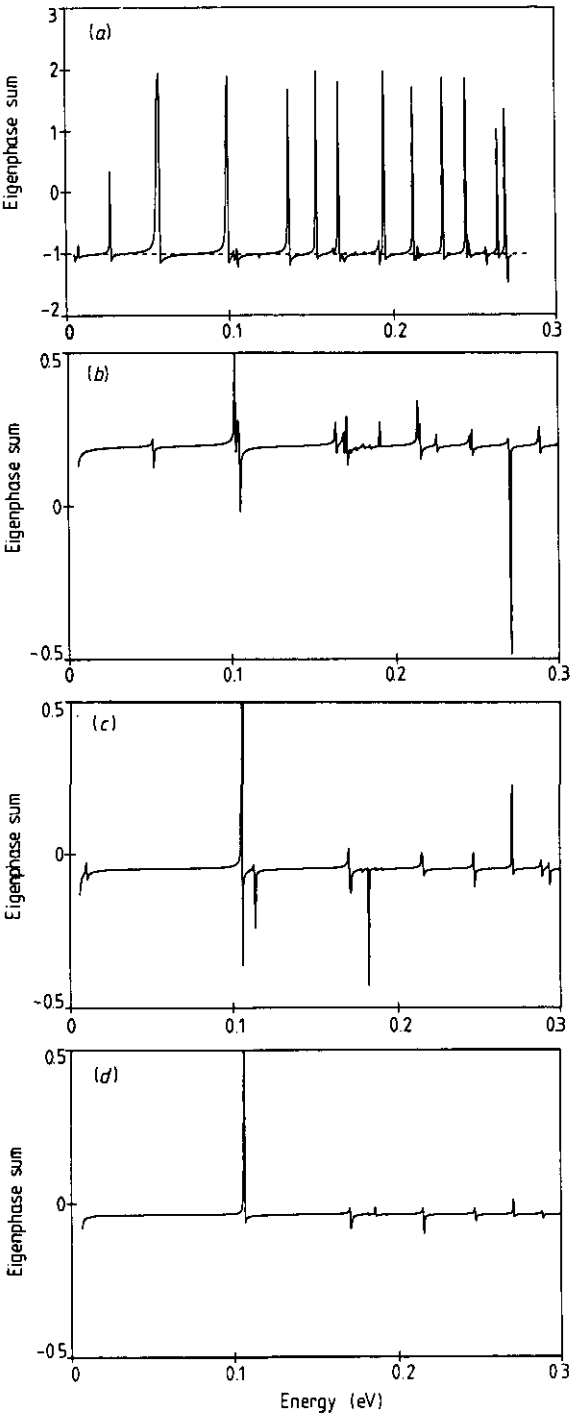

Figure 2. Eigenphase sums below the first vibrational threshold (not shown in figure). The full curve depicts the non-adiabatic eigenphase sum and the broken line depicts the eigenphase sum at the fixed equilibrium geometry ($R_e = 1.455$). (*a*) Σ; (*b*) Π; (*c*) Δ; (*d*) Φ.

where Γ is the width of the resonance in rydbergs. The non-adiabatic MCQD parameters are tabulated in table 3 for the four symmetries considered. The approximate l labelling has been made using the eigenvector compositions and corresponds to the dominant component. The eigenvector compositions suggest appreciable mixing for the higher l states.

Table 3. MCQD parameters just above the ground state and first vibrational threshold. The subscripts on α and β denote the threshold above which the parameters have been calculated. Powers of ten in parentheses.

	Σ			Π		
l	α_0	α_1	β_1	α_0	α_1	β_1
0	0.101	0.132	2.90(−3)			
1	−0.456	−0.402	1.35(−3)	0.040	0.041	3.45(−4)
2	0.028	0.036	3.66(−4)	0.016	0.019	1.93(−4)
3	0.007	0.009	1.98(−4)	0.006	0.007	1.77(−4)
4	0.001	0.002	1.55(−4)	0.000	0.001	1.51(−4)
5	−0.005	−0.005	5.67(−5)	−0.005	−0.005	6.55(−5)
	Δ			Φ		
l	α_0	α_1	β_1	α_0	α_1	β_1
2	−0.015	−0.013	2.01(−4)			
3	−0.006	0.005	1.34(−4)	−0.009	−0.008	1.42(−4)
4	0.004	−0.001	9.93(−5)	0.001	0.001	6.99(−5)
5	−0.002	−0.005	7.02(−5)	−0.005	−0.005	3.02(−5)

Table 4. Energy and other parameters for the resonances below first vibrational threshold, for Σ symmetry. The effective quantum number, n^*, and β calculated relative to the $v = 1$ threshold are tabulated in columns 3 and 4 respectively. Columns 6 and 7 tabulate these quantities relative to the correct threshold if different from $v = 1$. Powers of ten in parentheses.

Energy (eV)	Width (eV)	n^*	β	Assignment	n^*	β
0.0279	1.5(−4)	6.188	6.5(−4)	4p $^2\Sigma$, $v = 2$	4.406	2.4(−4)
0.0552	7.9(−4)	6.444	3.9(−3)	6p $^2\Sigma$, $v = 1$		
0.0982	5.7(−4)	6.910	3.5(−3)	7s $^2\Sigma$, $v = 1$		
0.1359	3.9(−4)	7.416	3.0(−3)	7p $^2\Sigma$, $v = 1$		
0.1595	1.9(−4)	7.671	1.6(−3)	5s $^2\Sigma$, $v = 2$	4.889	4.1(−4)
0.1662	2.6(−4)	7.917	2.4(−3)	8s $^2\Sigma$, $v = 1$		
0.1915	1.4(−4)	8.426	1.4(−3)	3p $^2\Sigma$, $v = 4$	3.493	1.1(−4)
0.1939	1.9(−5)	8.478	2.2(−3)	8p $^2\Sigma$, $v = 1$		
0.2119	2.2(−4)	8.913	2.9(−3)	9s $^2\Sigma$, $v = 1$		
0.2141	3.4(−5)	8.969	4.5(−4)	9d $^2\Sigma$, $v = 1$		
0.2302	2.0(−4)	9.433	3.1(−3)	9p $^2\Sigma$, $v = 1$		
0.2445	1.6(−4)	9.906	2.9(−3)	10s $^2\Sigma$, $v = 1$		

Tables 4–6 give a quantum defect analysis (Seaton 1983) of the resonances in the non-adiabatic eigenphase sum, figure 2. The resonances have been detected and

Table 5. As in table 4; Π symmetry resonances.

Energy (eV)	Width (eV)	n^*	β	Assignment	n^*	β
0.0522	2.5(−5)	6.411	1.2(−4)	$^2\Pi$		
0.1021	4.9(−5)	6.957	3.2(−4)	7p $^2\Pi$, $v = 1$		
0.1043	3.1(−5)	6.984	2.0(−4)	7d $^2\Pi$, $v = 1$		
0.1053	2.4(−6)	6.997	1.5(−4)	7f $^2\Pi$, $v = 1$		
0.1635	3.0(−5)	7.869	2.6(−4)	4p $^2\Pi$, $v = 3$	3.948	3.4(−5)
0.1684	2.3(−5)	7.959	2.2(−4)	8p $^2\Pi$, $v = 1$		
0.1696	2.2(−5)	7.982	2.2(−4)	8d $^2\Pi$, $v = 1$		
0.2137	2.3(−5)	8.958	3.1(−4)	9p $^2\Pi$, $v = 1$		
0.2152	1.6(−5)	8.999	2.3(−4)	9f $^2\Pi$, $v = 1$		
0.2254	1.6(−5)	9.284	2.4(−4)	$^2\Pi$		
0.2459	1.6(−5)	9.958	3.1(−4)	10p $^2\Pi$, $v = 1$		

Table 6. As in table 4; Δ and Φ symmetry resonances.

Energy (eV)	Width (eV)	n^*	β	Assignment	n^*	β
0.1054	3.8(−5)	6.998	2.4(−4)	7g $^2\Delta$, $v = 1$		
0.1061	3.4(−5)	7.006	2.1(−4)	7f $^2\Delta$, $v = 1$		
0.1136	2.3(−5)	7.103	1.5(−4)	7d $^2\Delta$, $v = 1$		
0.1703	1.5(−5)	7.995	1.4(−4)	8g $^2\Delta$, $v = 1$		
0.1822	4.2(−6)	8.229	4.4(−5)	5f $^2\Delta$, $v = 2$	4.990	9.6(−6)
0.1908	2.4(−6)	8.411	2.7(−5)	4d $^2\Delta$, $v = 3$	4.011	2.9(−6)
0.2471	1.6(−5)	10.000	2.9(−4)	10d $^2\Delta$, $v = 1$		
0.1057	1.9(−5)	7.001	1.2(−4)	7g $^2\Phi$, $v = 1$		
0.1061	2.2(−5)	7.007	1.4(−4)	7f $^2\Phi$, $v = 1$		
0.1858	5.7(−6)	8.302	6.0(−5)	5f $^2\Phi$, $v = 2$	5.006	1.3(−5)
0.2154	8.7(−6)	9.007	1.2(−4)	9f $^2\Phi$, $v = 1$		
0.2471	7.5(−6)	10.001	1.4(−4)	10g $^2\Phi$, $v = 1$		
0.2472	7.8(−6)	10.007	1.4(−4)	10f $^2\Phi$, $v = 1$		

fitted to a Breit–Wigner form using a program by Tennyson and Noble (1984) using an energy mesh of 2×10^{-5} Ryd. Because the resonances are very narrow and the eigenphase sum is flat between resonances a constant background was used for each fit.

The structure in the non-adiabatic eigenphase can be appreciated by noting that there are many Rydberg states of the neutral molecule converging on the target state, X $^1\Sigma$. Each Rydberg state has its own vibrational spectrum, see figure 3. Those vibrational states which lie above the HeH^+ ($v = 0$) state show up as resonances in the scattering cross section. Of course there should be an infinite number of Rydberg series, but because we have used $l \leq 5$ only those up to h wave are actually included in the calculation. These resonances are described as 'nuclear-excited Feshbach' resonances and are similar to 'core-excited Feshbach' resonances except that excitation of the nuclear rather than electronic motion is involved. Such resonances must occur for any positively charged molecular ion which has a potential well deep enough to support more than one vibrational bound state.

We find clear indications of Rydberg series in our results for vibrationally elastic

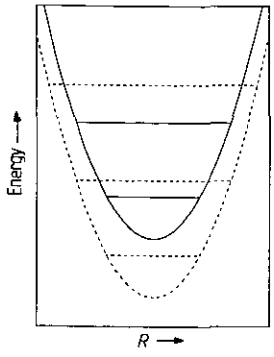

Figure 3. Schematic diagram showing the typical potential energy curve and vibrational levels of an bound ion state (——) and an associated high Rydberg state (– – –) of the neutral molecule.

scattering, tables 4–6. This is most obvious for the $^2\Pi$ symmetry where the 7p, 8p, 9p and 10p states are easily picked out. The assignments in tables 4–6 have been made using the MCQD parameters in table 3, the first label, e.g. '7p', denotes the state of hydrogen to which the energy levels correlates in the limit of infinite separation. The assignments are further confirmed by comparison with our bound state calculations (Sarpal *et al* 1991). Some of the features in our eigenphase plots were not accurately fitted and these have been omitted from the table. This is apparent in the large increments in the effective quantum numbers for the Δ and Φ symmetry results. This is due to the overlapping of higher angular momentum resonances which could be partly overcome by using a finer energy mesh.

The $^2\Sigma$ resonance at 0.055 eV, table 4, is clearly associated with the Rydberg state 6p $^2\Sigma$ with $v = 1$. It has a quantum defect of -0.444, close to the quantum defects of 2p, 3p, 4p and 5p bound states. The resonance at 0.027 eV is a little difficult to interpret by the prescription outlined so far. It has a quantum defect of -0.188 relative to $v = 1$ threshold, unlike any of our $^2\Sigma$ bound states. This resonance can only be interpreted correctly if it is associated with the second vibrational threshold, i.e. $v = 2$, resulting in an effective quantum number of 4.406. We therefore assign this resonance to be the 4p $^2\Sigma$ and $v = 2$ bound state of HeH. Such a conclusion is further supported by the difference in widths of the two resonances at 0.027 and 0.055 eV, see table 4, $\Delta v = 1$ coupling being stronger than that for $\Delta v = 2$.

There are two resonances in table 5 which we have not been able to assign. These resonances appear to be high-l states which have been shifted up in energy possibly by interaction with vibrationally excited states converging to higher vibrational thresholds, not explicitly included in our calculations.

The resonance structure observed for vibrationally elastic scattering, figure 2 and table 4, corresponds to the resonances observed by Yousif and Mitchell (1989) in the DR cross section. Our first resonance at 0.028 eV (4p $^2\Sigma$, $v = 2$) coincides with their deep resonance at 0.027 eV. However their cross section does not fully resolve a resonance where we calculate our second resonance (6p $^2\Sigma$, $v = 1$), 0.055 eV, but their results show a significant dip at this energy. Yousif and Mitchell also observe a sudden drop in their DR cross section at 0.1 eV. Our results suggest that this is due to the clustering of higher Rydberg states of the neutral molecule below the first vibrational threshold of the ion just below 0.4 eV, see figure 2.

3.3. Vibrational excitations

The adiabatic vibrational excitations from the lowest five levels are given in figures 4 and 5. The cross sections show a sharp rise at threshold, which is normally the case for positively charged ions, and then decay slowly. For vibrational excitations the convergence with total symmetry, Λ, is somewhat slower than for elastic scattering. The higher symmetry partial waves contribute a relatively larger proportion of the total excitation cross section at high energies and increasing with the vibrational quantum number v. For example for the $v = 0 \rightarrow 1$ transition the $1 \leq \Lambda \leq 3$ symmetries contribute 12% of the 'total' vibrational cross section at threshold, whereas for the $v = 4 \rightarrow 5$ transition it is as much as 37%. Figure 4 shows the convergence for the $v = 0 \rightarrow 1$ cross section. Conservative estimates suggest that our lowest cross section is converged to within 5% and the higher cross sections to within 10%. Excitation cross sections for transitions with $\Delta v = 2$ are an order of magnitude smaller than those for the corresponding $\Delta v = 1$ transition.

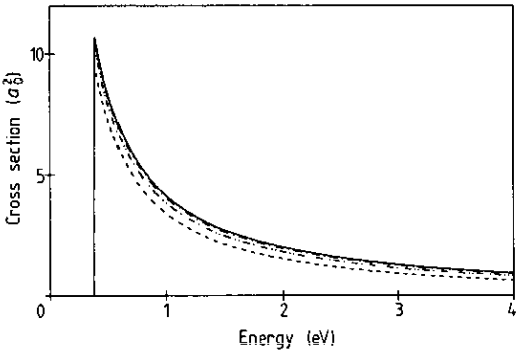

Figure 4. Adiabatic vibrational excitation cross sections for $v = 0 \rightarrow 1$. – – –, Σ; – ·· – ·· –, $\Sigma + \Pi$; – · – · –, $\Sigma + \Pi + \Delta$; and —— $\Sigma + \Pi + \Delta + \Phi$.

The $v \rightarrow v + 1$ cross sections rise with increasing vibrational quantum number, v, of the lower state. The Coulomb–Born expression for the cross section (see for example Boikova and Ob'edkov 1968) includes the factor $v + 1$. In our adiabatic calculations ($\Lambda = 0$) the threshold cross sections are in the ratio 1 : 1.9 : 2.7 : 3.6 : 4.7 for upper vibrational quantum numbers 1, 2, 3, 4 and 5 respectively. The corresponding ratio for our total cross sections ($\Lambda \leq 3$) is 1 : 2.06 : 3.25 : 4.73 : 6.75. This suggests that the Coulomb–Born cross sections provide a good qualitative description of the excitation cross section, but the quantitative results are found to differ quite appreciably. Comparison with the results of Boikova and Ob'edkov (1968) shows that their Coulomb–Born cross section at threshold is more than double our adiabatic cross section for the $v = 0 \rightarrow 1$ excitation, and is consistently higher throughout the energy range.

Boikova and Ob'edkov's (1968) modified Coulomb–Born calculations, which explicitly include the dipole and quadrupole moments of the ion, assume that the vibrational excitations are dominated by the long-range interactions of the electron. We however observe no evidence for this in our results. We were able to control the interactions in the outer region in our calculations and found that cross sections were not significantly altered by removing the dipole and quadrupole terms in the potential.

Although low-energy rotational excitations are certainly dominated by long-range

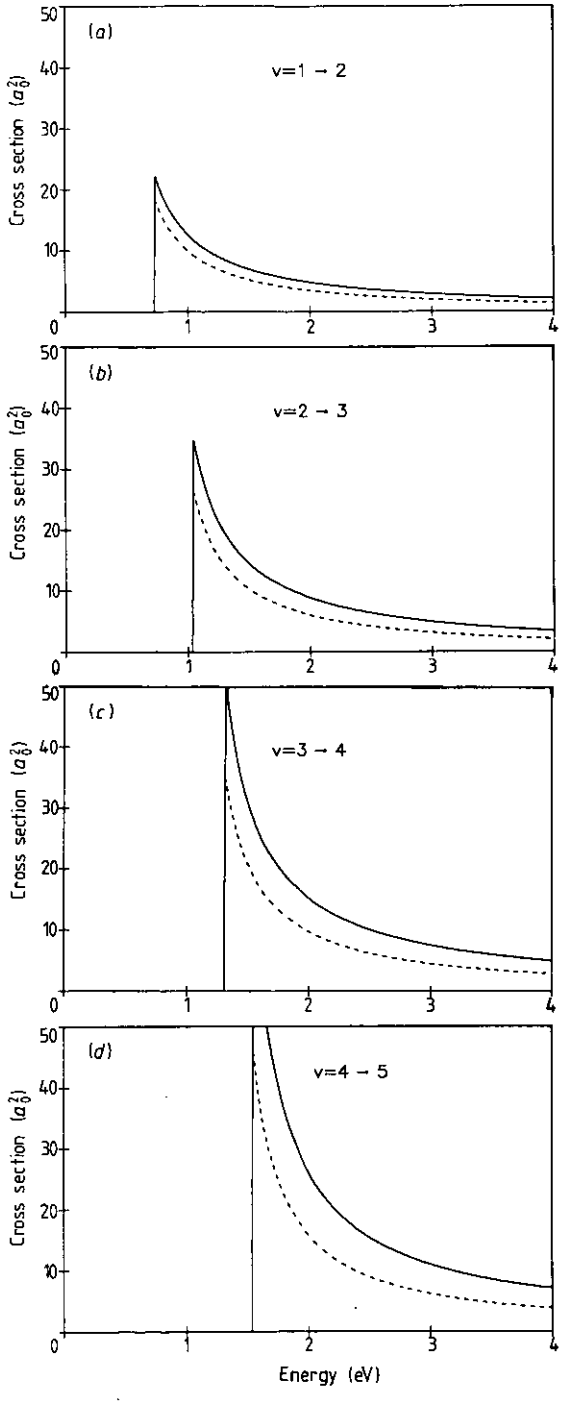

Figure 5. Adiabatic vibrational cross sections, (*a*) $v = 1 \rightarrow 2$; (*b*) $v = 2 \rightarrow 3$; (*c*) $v = 3 \rightarrow 4$; (*d*) $v = 4 \rightarrow 5$. Broken curves denote Σ cross sections only, full curves denote sum of cross sections up to Φ.

interactions (Dalgarno and Henry 1965) this is not the case for vibrational excitations (Lane 1980). The divergence of the dipole term in the potential at short distances and the neglect of short-range interactions, particularly exchange, probably explain why Boikova and Ob'edkov (1968) obtain vibrational excitation cross sections which are considerably larger than ours. The modified Coulomb–Born approximation is really only valid for low-energy vibrational excitations when long-range interactions are dominant. The short-range interactions, by which we mean interactions within the R-matrix sphere, act as damping terms and play a significant role in the excitation mechanism for HeH^+ (and possibly for positive ions in general).

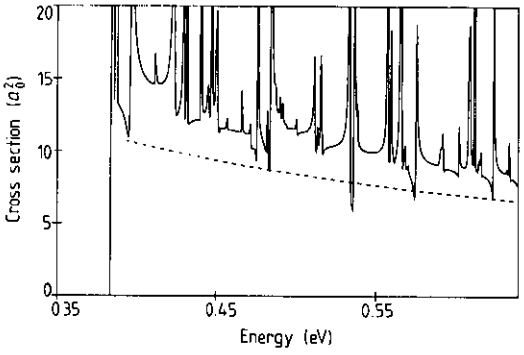

Figure 6. Total non-adiabatic $v = 0 \rightarrow 1$ cross section; the broken curve shows the total adiabatic cross section of figure 4.

When non-adiabatic effects are included the vibrational excitation cross section is considerably different from the adiabatic results at low energies, see figure 6. Although the general trend of the cross section follows that of the adiabatic results, with the non-adiabatic cross section converging to the adiabatic cross sections for sufficiently high energies, there is considerable structure in the non-adiabatic results which is completely absent from our adiabatic calculations. These resonances are extremely narrow ($< 10^{-4}$ Ryd) and it would thus require very high resolution to observe them experimentally. We omit a detailed analysis of the resonance structure and simply remark that the origin of such resonances must be the vibronic states of the neutral molecule, as in the elastic channel.

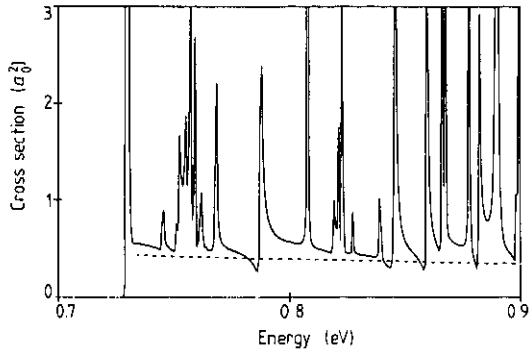

Figure 7. Total non-adiabatic $v = 0 \rightarrow 2$ cross section; the broken curve shows the total adiabatic cross section.

The convergence of the cross section with respect to Λ for the non-adiabatic calculations is similar to our adiabatic results, however a somewhat larger contribution is made by the higher symmetries, see figure 6. In going from the adiabatic to the non-adiabatic approximation we observe a transfer of flux from the elastic channel to the inelastic ones, resulting in higher vibrational excitation cross sections for Π and higher symmetries. Nevertheless we estimate our $v = 0 \rightarrow 1$ cross section to have converged to within 5%. As with our adiabatic calculations the $v = 0 \rightarrow 2$ cross sections are an order of magnitude smaller than the corresponding $v = 0 \rightarrow 1$ cross sections, see figure 7.

4. Conclusions

We have explored the breakdown of the Born–Oppenheimer approximation for low-energy collisions between electrons and HeH^+ in regions close to resonances and shown that it is the cause of the observed structure in the dissociative recombination cross section measured by Yousif and Mitchell (1989). We have been able to assign these resonances by our *ab initio* calculations and to estimate their positions accurately.

We have shown that a rigorous treatment of the scattering process produces vibrational excitation cross sections considerably smaller than those using the Coulomb–Born approximation. Although the non-adiabatic cross sections are larger than the adiabatic results they are still significantly smaller than those calculated using the Coulomb–Born approximation. Since the principal astrophysical excitation mechanism of HeH^+ is considered to be electron impact, the lower cross sections may perhaps explain why the emissions infrared spectrum of HeH^+ has not been measured in planetary nebulae (Moorhead *et al* 1988).

The absence of curve crossing and significant DR for non-resonant scattering, points to a clear breakdown of the Born–Oppenheimer approximation for low energies. Clearly proper account must be taken of the various competing channels for an accurate treatment of dissociative recombination. Work is in progress using the present calculations to give dissociative recombination cross sections and also extending them to high-energy scattering which can result in dissociation to excited states of the atomic constituents. Both studies will be reported at a later date.

Acknowledgments

We would like to thank Charles Gillan for help with calculating target moments and Susan Branchett for helpful discussions during the course of this work. This work was supported by SERC grant GR/F/14550.

References

Boikova R F and Ob'edkov V D 1968 *Sov. Phys.–JETP* **27** 772–4

Collins L A, Schneider B I, Noble C J, McCurdy C W and Yabushita S 1986 *Phys. Rev. Lett.* **57** 980–3

Dabrowski I and Herzberg G 1977 *Trans. NY Acad. Sci.* **38** 14–25

Dalgarno A and Henry R J W 1965 *Proc. Phys. Soc.* **85** 679–84

Gillan C J, Nagy O, Burke P G, Morgan L A and Noble C J 1987 *J. Phys. B: At. Mol. Phys.* **20** 4585–603

Green T A, Michels H H, Browne J C and Madsen M M 1974 *J. Chem. Phys.* **61** 5186–97
Green T A, Michels H H, and Browne J C 1978 *J. Chem. Phys.* **69** 101–5
Ketterle W 1989 *Phys. Rev. Lett.* **62** 1480–3
Lane N F 1980 *Rev. Mod. Phys.* **52** 29–119
McLean A D 1971 *Conf. Potential Energy Surfaces in Chemistry* ed W A Lester Jr (San Jose: IBM Research Laboratory) p 87
Michels H H 1989 *Dissociative Recombination: Theory, Experiment and Applications* ed J B A Mitchell and S L Guberman (World Sceintific: Singapore) pp 97–108
Mitchell J B A 1990 *Phys. Rep.* **186** 215–48
Moorhead J M, Lowe R P, Maillard J P, Wehlau W H and Bernath P F 1988 *Astrophys. J.* **326** 899-904
Morgan L A 1984a *Computer Phys. Commun.* **31** 419–22
—— 1984b *J. Phys. B: At. Mol. Phys.* **19** L439–45
—— 1990 *Proc. 16th Int. Conf. on Physics of Electronic and Atomic Collisions* ed A Dalgarno, R S Freund M S Lubell and T B Lucatorto (Plenum: New York) Invited Papers and Progress Reports pp 96–102
Morgan L A and Burke P G 1988 *J. Phys. B: At. Mol. Opt. Phys.* **21** 2091–105
Morgan L A, Burke P G and Gillan C J 1990 *J. Phys. B: At. Mol. Opt. Phys.* **23** 99–113
Noble C J 1982 *Daresbury Laboratory Technical Memorandum* DL/SCI/TMT33T
Noble C J and Nesbet R K 1984 *Comput. Phys. Commun.* **33** 399–411
Peyerimhoff S D 1965 *J. Chem. Phys.* **43** 998–1010
Raseev G and Le Rouzo H 1983 *Phys. Rev.* A **27** 268–84
Roberge W and Dalgarno A 1982 *Astrophys. J.* **255** 489–96
Sarpal B K, Branchett S E, Tennyson J and Morgan L A 1991 to be published
Schneider B I, Le Dourneuf M and Burke P G 1979 *J. Phys. B: At. Mol. Opt. Phys.* **40** L365–9
Seaton M J 1983 *Rep. Prog. Phys.* **46** 167–257
—— 1985 *J. Phys. B: At. Mol. Phys.* **18** 2111–31
Tennyson J 1988 *J. Phys. B: At. Mol. Opt. Phys.* **21** 805–16
Tennyson J, Burke P G and Berrington K A 1987 *Comput. Phys. Commun.* **47** 207–12
Tennyson J and Noble C J 1984 *Comput. Phys. Commun.* **32** 421–4
Tennyson J, Noble C J and Burke P G 1986 *Int. J. Quantum Chem.* **29** 1033–42
Theodorakopoulos G, Farantos S C, Buenker R J and Peyerimhoff S D 1984 *J. Phys. B: At. Mol. Phys.* **17** 1453–62
Yousif F B and Mitchell J B A 1989 *Phys. Rev. A* **40** 4318–21